Letter

Theory of magnetic field stabilized compact skyrmions in thin-film ferromagnets

Anne Bernand-Mantel,[1,2,*] Anaïs Fondet,[1,2] Sarah Barnova,[1] Theresa M. Simon,[3] and Cyrill B. Muratov[4,5]

[1]*Université de Toulouse, Laboratoire de Physique et Chimie des Nano-Objets, UMR 5215 INSA, CNRS, UPS, 135 Avenue de Rangueil, F-31077 Toulouse Cedex 4, France*

[2]*Centre d'Elaboration de Matériaux et d'Etudes Structurales, CEMES-CNRS, 29 rue Jeanne Marvig, 31055 Toulouse, France*

[3]*Institut für Analysis und Numerik, Westfälische Wilhelms-Universität Münster, Einsteinstr. 62, 48149 Münster, Germany*

[4]*Department of Mathematical Sciences, New Jersey Institute of Technology, Newark, New Jersey 07102, USA*

[5]*Departimento di Matematica, Università di Pisa, Largo B. Pontecorvo, 5, 56127 Pisa, Italy*

(Received 2 June 2023; revised 18 September 2023; accepted 19 September 2023; published 13 October 2023)

We present a micromagnetic theory of compact magnetic skyrmions under applied magnetic field that accounts for the full dipolar energy and the interfacial Dzyaloshinskii-Moryia interaction (DMI) in the thin-film regime. Asymptotic analysis is used to derive analytical formulas for the parametric dependence of the skyrmion size and rotation angle, as well as the energy barriers for collapse and bursting, two processes that lead to a finite skyrmion lifetime. We demonstrate the existence of a regime at low DMI, in which the skyrmion is stabilized by a combination of nonlocal dipolar interaction and a magnetic field applied parallel to its core, and discuss the conditions for an experimental realization of such field-stabilized skyrmions.

DOI: 10.1103/PhysRevB.108.L161405

Introduction. Since the first real-space observation of skyrmions in a chiral magnet [1], there have been a great number of theoretical and experimental studies devoted to skyrmionics [2,3]. These developments are motivated by the remarkable compactness, stability, and tunability of skyrmions, which makes them attractive candidates for future applications in information technology [3,4]. Starting with the first experiments in chiral magnets [1], it was observed that skyrmions spontaneously appear in a certain range of nonzero magnetic field in various bulk materials and thin-film heterostructures [5]. Indeed, while the ground state of chiral magnets is the helical state at zero magnetic field, the ferromagnetic ground state is restored when a sufficiently strong magnetic field is applied. However, isolated skyrmions and skyrmion lattices may exist as metastable states under applied magnetic fields, as predicted in the late 1980s [6,7]. The precise dependence of an isolated skyrmion size on the applied magnetic field was investigated numerically [7–10]. In the isolated skyrmion regime, the size of a skyrmion decreases (increases) with increasing (decreasing) magnetic field applied antiparallel to the magnetization in the skyrmion core [7,9].

While the antiparallel configuration has been widely investigated theoretically and experimentally [5,11–21], the parallel configuration was considered in only a handful of studies [9,10,22,23]. The reason is that most studies on skyrmions are carried out in the strong Dzyaloshinskii-Moryia interaction (DMI) regime, where isolated skyrmions are very easily destabilized by a magnetic field applied parallel to the skyrmion core via the so-called "bursting" phenomenon, whereby the magnetic layer is reversed to the uniform state as the skyrmion radius goes to infinity. The position of the bursting line on the skyrmion stability diagram was estimated by numerical minimization in previous theoretical works [9,10,22,23]. A solution to avoid this instability is to confine the skyrmion in a dot to extend its stability to a wider range of applied fields [24–26]. Another possibility is to work in the low DMI regime. In this regime, it was recently demonstrated [27] that the nonlocal dipolar interaction that has been classically neglected [9,10,28], may become comparable to the DMI and play a role in skyrmion stabilization. Several works based on approximate models suggest that the nonlocal dipolar interaction modifies the range of existence of isolated skyrmions in applied magnetic fields [22,23], but this regime has remained largely unexplored.

In this Letter, we carry out an investigation of isolated compact skyrmions under an applied magnetic field in the thin-film and low DMI regime, taking into account the full stray field. We carry out an asymptotic analysis and obtain analytical formulas predicting the skyrmion radius, angle, as well as the collapse and bursting energy barriers as functions of the system parameters. We obtain a skyrmion stability diagram, which reveals a different response to a parallel field at low DMI strength compared to the existing phase diagrams [10,22,23]. This modification of the skyrmion phase diagram due to stray field effects is confirmed by direct micromagnetic simulations. We emphasize that in this regime the parallel field enables one to increase the skyrmion size and stability and discuss possible routes to observe field-stabilized skyrmions experimentally in conventional skyrmion materials.

Model. We consider a ferromagnetic thin film with perpendicular magnetic anisotropy and interfacial DMI. Following our previous works [27,29–31] with the addition

*bernandm@insa-toulouse.fr

of the Zeeman energy term, the micromagnetic energy of a magnetization $\mathbf{m}:\mathbb{R}^2\to\mathbb{S}^2$ reduces to (see Supplemental Material [32] for details and the references [33–36] therein)

$$\begin{aligned}E(\mathbf{m}) = &\int_{\mathbb{R}^2}(|\nabla\mathbf{m}|^2+(Q-1)|\mathbf{m}_\perp|^2)d^2r\\ &-\int_{\mathbb{R}^2}[2h(m_\parallel+1)+2\kappa\mathbf{m}_\perp\cdot\nabla m_\parallel]\,d^2r\\ &-\frac{\delta}{8\pi}\int_{\mathbb{R}^2}\int_{\mathbb{R}^2}\frac{[m_\parallel(\mathbf{r})-m_\parallel(\mathbf{r}')]^2}{|\mathbf{r}-\mathbf{r}'|^3}\,d^2r\,d^2r'\\ &+\frac{\delta}{4\pi}\int_{\mathbb{R}^2}\int_{\mathbb{R}^2}\frac{\nabla\cdot\mathbf{m}_\perp(\mathbf{r})\nabla\cdot\mathbf{m}_\perp(\mathbf{r}')}{|\mathbf{r}-\mathbf{r}'|}\,d^2r\,d^2r',\end{aligned}\tag{1}$$

where $\mathbf{m}_\perp\in\mathbb{R}^2$ is the in-plane component of $\mathbf{m}$, i.e., the component perpendicular to the out-of-plane anisotropy easy axis, and $m_\parallel\in\mathbb{R}$ is the out-of-plane component of $\mathbf{m}$, i.e., the component parallel to the easy axis. The energy is measured in the units of Ad, where A is the exchange stiffness and d the film thickness. Lengths are measured in the units of the exchange length $\ell_{\rm ex}=\sqrt{2A/(\mu_0M_{\rm s}^2)}$, where $M_{\rm s}$ is the saturation magnetization and μ_0 the vacuum magnetic permeability. The dimensionless film thickness is $\delta=d/\ell_{\rm ex}\lesssim 1$. We assume that the external magnetic field is applied normally to the film plane. We introduced the dimensionless quality factor $Q=K_{\rm u}/K_{\rm d}>1$, where $K_{\rm u}$ is the magnetocrystalline anisotropy constant and $K_{\rm d}=\frac{1}{2}\mu_0M_{\rm s}^2$, the dimensionless DMI strength $\kappa=D/\sqrt{AK_{\rm d}}$, and the dimensionless applied magnetic field h defined as $h=(\mathbf{H}\cdot\hat{\mathbf{z}})/M_{\rm s}$. The first four energy terms are local and represent, respectively, the exchange energy, the effective anisotropy energy (magnetocrystalline energy renormalized to take into account the local stray field contribution), the Zeeman energy, and the DMI energy. The last two terms correspond to the long-range part of the dipolar energy, which splits into surface and volume contributions (see [32] for details).

We are considering an isolated skyrmion with a magnetization pointing up in its center, in a background where the magnetization is pointing down. As a consequence, we assume that the applied magnetic field in the positive field direction is lower than the anisotropy field, $h<Q-1$, to ensure that the uniform state $\mathbf{m}_0=-\hat{\mathbf{z}}$ is a local minimizer of the energy. Under the condition that $\mathbf{m}(\mathbf{r})\to-\hat{\mathbf{z}}$ sufficiently fast as $|\mathbf{r}|\to\infty$, we consider the skyrmion number $q(\mathbf{m})=\frac{1}{4\pi}\int_{\mathbb{R}^2}\mathbf{m}\cdot(\frac{\partial\mathbf{m}}{\partial x}\times\frac{\partial\mathbf{m}}{\partial y})dx\,dy$ [18,37], so that with our convention we have $q(\mathbf{m})=1$ for a skyrmion profile.

Skyrmion profiles. In the regime, in which the other energy terms remain perturbations to the dominating exchange energy, the skyrmion profile can be shown to be close to a Belavin-Polyakov profile [38], i.e., a minimizer of the exchange energy among all $\mathbf{m}$ with $q(\mathbf{m})=1$ [39]. Therefore, we can proceed as in [27,38] with an asymptotic analysis based on a suitably truncated Belavin-Polyakov type profile $\mathbf{m}_{\rho,\theta,L}$ (for the precise form, see [32]), with the necessary modifications to account for the presence of the applied field. The equilibrium radius ρ, the rotation angle θ, and the cutoff scale L are obtained [32,38] from the minimization of the

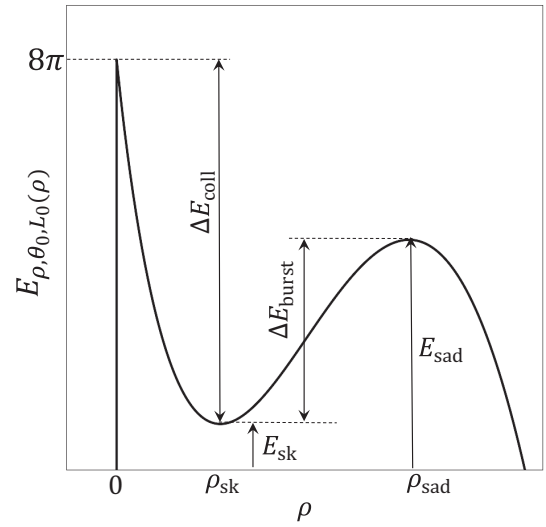

FIG. 1. Leading order skyrmion energy $E_{\rho,\theta,L}$ vs radius ρ after minimization over θ and L for $\kappa=0.35$, $\delta=0.7$, $h=0.008$, and $Q=1.591$ [see (2.27) in the Supplemental Material [32]].

leading order energy $E(\mathbf{m}_{\rho,\theta,L})\simeq E_{\rho,\theta,L}$, where (see Fig. 1 for an illustration)

$$\begin{aligned}E_{\rho,\theta,L} = &\,8\pi+\frac{4\pi}{L^2}+4\pi(Q-1-h)\rho^2\ln\left(\frac{4L^2}{e^{2(1+\gamma)}}\right)\\ &-4\pi h\rho^2-8\pi\kappa\rho\,\cos\theta+\frac{\pi^3\rho\delta}{8}(3\,\cos^2\theta-1),\end{aligned}\tag{2}$$

where $\gamma\approx 0.5772$ is the Euler-Mascheroni constant. Under the assumption $\bar{\varepsilon}\ll 1$, where

$$\bar{\varepsilon}=\frac{1}{\sqrt{1-\bar{h}}}\times\begin{cases}\left(8\pi|\bar{\kappa}|-\frac{\pi^3}{4}\bar{\delta}\right) & \text{if } |\bar{\kappa}|\geqslant\frac{3\pi^2}{32}\bar{\delta},\\ \left(\frac{128\bar{\kappa}^2}{3\pi\bar{\delta}}+\frac{\pi^3}{8}\bar{\delta}\right) & \text{else,}\end{cases}\tag{3}$$

with

$$\bar{\delta}=\frac{\delta}{\sqrt{Q-1}},\quad \bar{\kappa}=\frac{\kappa}{\sqrt{Q-1}},\quad \bar{h}=\frac{h}{Q-1},\tag{4}$$

the minimizer of the reduced energy in (2) gives the leading order skyrmion equilibrium angle

$$\theta_0=\begin{cases}0 & \text{if } \bar{\kappa}\geqslant\frac{3\pi^2}{32}\bar{\delta},\\ -\pi & \text{if } \bar{\kappa}\leqslant-\frac{3\pi^2}{32}\bar{\delta},\\ \pm\arccos\left(\frac{32\bar{\kappa}}{3\pi^2\bar{\delta}}\right) & \text{else,}\end{cases}\tag{5}$$

and radius $\rho_{\rm sk}=\bar{\rho}_{\rm sk}/\sqrt{Q-1}$, in units of $\ell_{\rm ex}$, where

$$\bar{\rho}_{\rm sk}=\frac{1}{16\pi\sqrt{1-\bar{h}}}\frac{\bar{\varepsilon}}{(-W_{-1}(-\beta\bar{\varepsilon}))},\tag{6}$$

provided that $\beta\bar{\varepsilon}<e^{-1}$ (see Sec. 2.3 in [32]). Here W_i refers to the ith real-valued branch of the Lambert W function [40], and $\beta=\frac{e^{1+\gamma}}{32\pi}\exp(\frac{\bar{h}}{2(1-\bar{h})})$. The energy of the optimal skyrmion solution is

$$E_{\rm sk}=8\pi-\frac{\bar{\varepsilon}^2}{32\pi W_{-1}^2(-\beta\,\bar{\varepsilon})}\left(-W_{-1}(-\beta\,\bar{\varepsilon})-\frac{1}{2}\right).\tag{7}$$

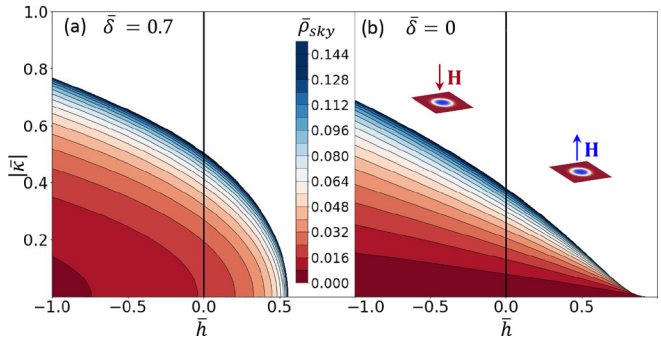

FIG. 2. Scaled skyrmion radius $\bar{\rho}_{\rm sk}$ for the intermediate thickness regime with $\bar{\delta} = 0.7$ (a) and ultrathin regime with $\bar{\delta} = 0$ (b) as a function of $\bar{\kappa}$ and $\bar{h}$. The convention for the field direction is shown schematically in the insets, where in the skyrmion image, the red and blue colors represent, respectively, down and up magnetizations and white corresponds to in-plane magnetization. For $\bar{h} < 0$, the field is applied antiparallel to the skyrmion core (red arrow in the inset), while for $\bar{h} > 0$ the field is parallel (blue arrow in the inset).

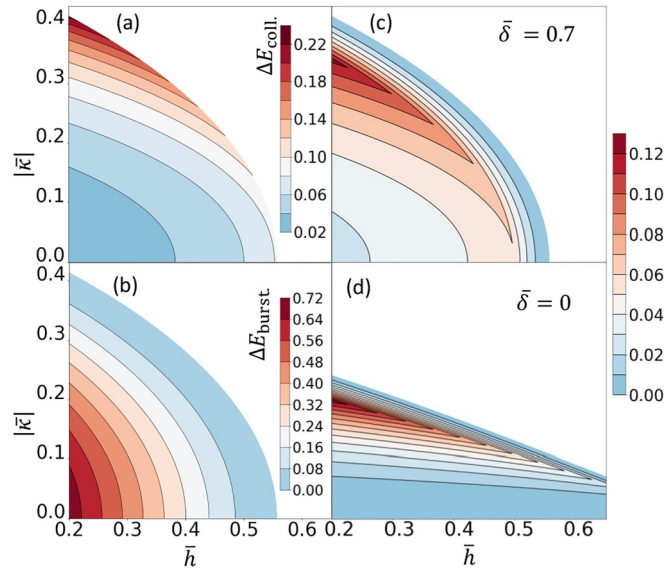

FIG. 3. Skyrmion collapse $\Delta E_{\rm coll}$ (a) and bursting $\Delta E_{\rm burst}$ (b) energy barriers (in units of Ad) for the intermediate thickness regime with $\bar{\delta} = 0.7$. Also shown is the effective barrier $\Delta E = \min(\Delta E_{\rm coll}, \Delta E_{\rm burst})$, which illustrates the optimal stability region against collapse and bursting for $\bar{\delta} = 0.7$ (c) and for the ultrathin film with $\bar{\delta} = 0$ (d).

For $0 < 1 - \bar{h} \ll 1$ with $\beta\bar{\varepsilon} < e^{-1}$ fixed, there is also a minimum energy saddle-point solution with equilibrium angle θ_0 from (5) and radius $\rho_{\rm sad} = \bar{\rho}_{\rm sad}/\sqrt{Q-1}$, where

$$\bar{\rho}_{\rm sad} = \frac{1}{16\pi\sqrt{1-\bar{h}}} \times \frac{\bar{\varepsilon}}{[-W_0(-\beta\bar{\varepsilon})]}. \tag{8}$$

The energy of the saddle is given by

$$E_{\rm sad} = 8\pi - \frac{\bar{\varepsilon}^2}{32\pi W_0^2(-\beta\,\bar{\varepsilon})}\left(-W_0(-\beta\,\bar{\varepsilon}) - \frac{1}{2}\right). \tag{9}$$

The above formulas become asymptotically exact when $\bar{\varepsilon} \to 0$ and $\bar{h} \to 1^-$ with $\beta\bar{\varepsilon}$ fixed, which corresponds to $\frac{\bar{\delta}+|\bar{\kappa}|}{\sqrt{1-\bar{h}}}\exp(\frac{1}{2(1-\bar{h})}) = O(1)$ as $\bar{\delta}, \bar{\kappa} \to 0$. Asymptotically, the skyrmion and the saddle-point solutions disappear via a saddle-node bifurcation at a critical value of $|\bar{\kappa}| = \bar{\kappa}_c$ given by

$$\bar{\kappa}_c = \begin{cases} \frac{\pi^2}{32}\bar{\delta} + \frac{4\sqrt{1-\bar{h}}}{e^{2+\gamma}}e^{-\bar{h}/[2(1-\bar{h})]} & \text{if } \bar{\delta} \leqslant \bar{\delta}_c, \\ \sqrt{\frac{3\pi^2\bar{\delta}}{4}\left(\frac{\sqrt{1-\bar{h}}}{e^{2+\gamma}}e^{-\bar{h}/[2(1-\bar{h})]} - \frac{\pi^2\bar{\delta}}{256}\right)} & \text{else,} \end{cases} \tag{10}$$

where $\bar{\delta}_c = \frac{64\sqrt{1-\bar{h}}}{\pi^2 e^{2+\gamma}}e^{-\bar{h}/[2(1-\bar{h})]}$, as the value of $|\bar{\kappa}|$ is increased.

Skyrmion phase diagram. In Fig. 2, we present the asymptotic skyrmion phase diagram by plotting the scaled skyrmion radius $\bar{\rho}_{\rm sk}$ from (6) as a function of the dimensionless DMI strength $\bar{\kappa}$ and applied field $\bar{h}$, where the positive field direction is parallel to the skyrmion core [see the insets in Fig. 2(b)]. Skyrmion solutions are predicted to exist when $0 < |\bar{\kappa}| + \bar{\delta} \lesssim 1$ and $\bar{h} \leqslant \bar{h}_c$, where $\bar{h}_c$ is obtained by solving for h in (10), while no skyrmion solutions are expected for $\bar{h} > \bar{h}_c$ (see also [32]).

According to Fig. 2, in the antiparallel configuration, $\bar{h} < 0$, the skyrmion radius is strongly increasing with $|\bar{\kappa}|$ and increasing slower with a decrease in $|\bar{h}|$. In the parallel configuration, $\bar{h} > 0$, in the intermediate thickness ($\bar{\delta} = 0.7$) regime shown in Fig. 2(a), the skyrmion radius dependence is, to the contrary, dominated by its magnetic field dependence and the dependence on $|\bar{\kappa}|$ is strongly reduced for small $|\bar{\kappa}|$. In particular, the lines of equal radius present a concave character and become parallel to the y axis as $|\bar{\kappa}| \to 0$. This diminished dependence of $\bar{\rho}_{\rm sk}$ on $|\bar{\kappa}|$ comes from the fact that the dominant stabilization mechanism in the low $|\bar{\kappa}|$ regime is the long-range dipolar interaction. The skyrmion behavior in this regime presents remarkable differences from what is predicted by the classical skyrmion theory, which only takes into account the local dipolar interaction [9,10,28]. For comparison, we set $\bar{\delta} = 0$ in our model in Fig. 2(b), which is equivalent to neglecting the long-range dipolar interactions. In this case, the lines of constant radius do not present this strong concave character and the main source of skyrmion stabilization in the whole field range is solely the increase of $|\bar{\kappa}|$.

Skyrmion stability. A second important outcome of our analysis is the prediction of the parametric dependence of the bursting energy barrier. Previous studies on skyrmion stability have focused on the collapse phenomenon and the field applied antiparallel to the skyrmion core [11,14,16,27,41–43]. However, for a field applied parallel to the skyrmion core, bursting is the main source of instability. These two energy barriers are shown in Fig. 1, where we present the skyrmion energy as a function of the radius ρ for a given set of parameters [see (2.27) in [32]]. The local minimum of energy at $\rho_{\rm sk}$ corresponds to the equilibrium skyrmion solution. For $\rho < \rho_{\rm sk}$ the energy is increasing with decreasing ρ and reaches the value 8π at $\rho = 0$, as all the energies tend to zero except the exchange energy, which tends to its minimum value of 8π among configurations with $q = 1$, as first demonstrated in [39] and discussed previously [11,14,23,27,38].

The energy difference between the equilibrium skyrmion and the "zero radius skyrmion" is thus $\Delta E_{\rm coll} = 8\pi - E_{\rm sk}$, which serves as the energy barrier to skyrmion collapse [44].

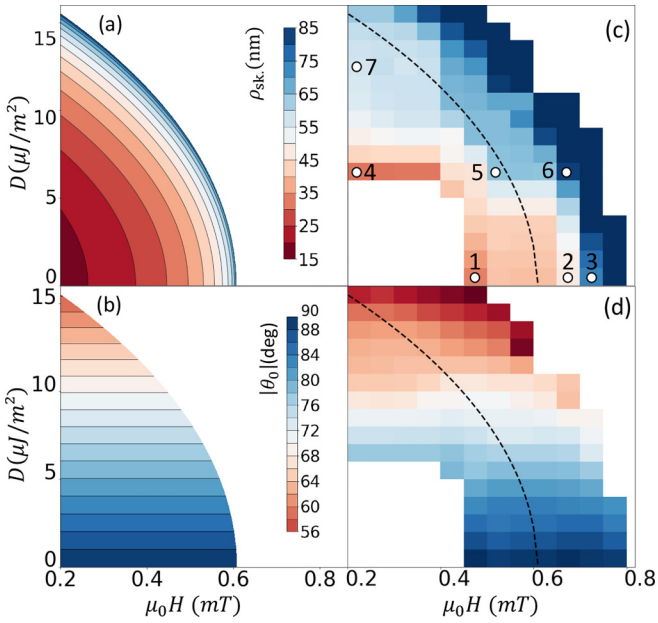

FIG. 4. The skyrmion characteristics in the low DMI regime for $d = 5$ nm, $A = 20$ pJ/m, $M_s = 10^5$ A/m, and $K_u = 6346$ J/m^3 corresponding to $Q = 1.01$: (a) skyrmion radius r_{sky} and (b) skyrmion rotation angle $|\theta_0|$ from (6) and (5); (c) skyrmion radius and (d) skyrmion rotation angle from MUMAX3 simulations on a 2048 × 2048 nm^2 square box with mesh size 2 × 2 × 5 nm. The dashed line is the line of zero bursting barrier defined in (10).

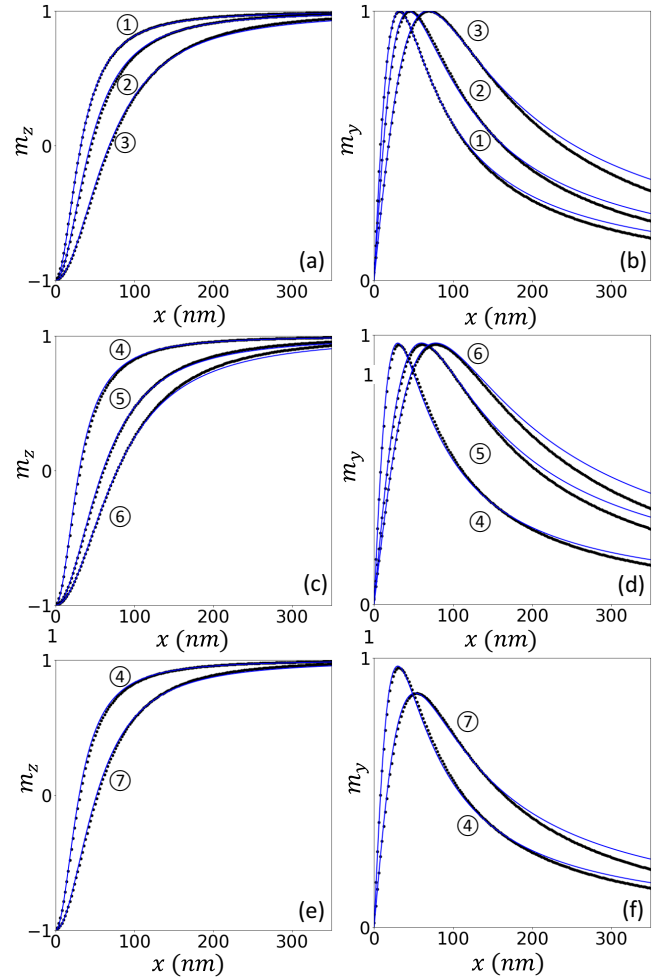

FIG. 5. The magnetization profiles along the x axis with the skyrmion at the origin obtained from the MUMAX3 simulations for the parameters indicated by the respective dots in Fig. 4(c). The simulation datapoints are shown with the solid black dots, while the Belavin-Polyakov profiles obtained by fitting their radius and angle to the simulation data are shown with the solid blue lines.

As the radius becomes larger than ρ_{sk}, the energy is increasing and a saddle point of the micromagnetic energy is observed at ρ_{sad}. This saddle prevents the skyrmion solution from bursting as the skyrmion energy would otherwise go to $-\infty$ as the skyrmion radius tends to infinity. The bursting barrier is defined as $\Delta E_{burst} = E_{sad} - E_{sk}$. The collapse and bursting energy barriers are plotted as functions of $|\bar{\kappa}|$ and $\bar{h}$ in Figs. 3(a) and 3(b) for the magnetic field applied parallel to the skyrmion core. The collapse and bursting energy barriers present opposite variations as the effective DMI or applied magnetic field are increased: an increase of $|\bar{\kappa}|$ or $\bar{h}$ increases the collapse barrier, but decreases the bursting barrier. As a consequence, in the positive field regime, our theory predicts that the optimum stability region for skyrmions is where both the collapse and the bursting barriers are large. This optimum stability region is illustrated in Figs. 3(c) and 3(d), where we plot the effective energy barrier $\Delta E = \min(\Delta E_{coll}, \Delta E_{burst})$. In Fig. 3(c), for an intermediate thickness ($\bar{\delta} = 0.7$), the optimal stability is obtained at large $|\bar{\kappa}|$, for low applied fields. As $|\bar{\kappa}|$ is decreased, the region of optimum stability, which appears in reddish colors, is shifted to positive fields, showing that the applied positive field can partly compensate the decrease of DMI to stabilize skyrmions in the low $|\bar{\kappa}|$ regime. The stabilization of the skyrmion in this regime is due to a combined effect of the applied positive field and the long-range dipolar interaction. In Fig. 3(d), we present the ultrathin film limit ($\bar{\delta} = 0$). In that case, the positive field cannot compensate the decrease of $|\bar{\kappa}|$ and hardly any increase of skyrmion stability with applied positive field is observed in the low $|\bar{\kappa}|$ regime. Comparison between these two cases in Figs. 3(c) and 3(d) reveals that the long-range dipolar interaction provides a stabilization mechanism in low DMI systems leading to a regime of parallel field stabilization of skyrmions.

Micromagnetic simulations. To confirm the existence of field-stabilized compact skyrmions in the positive field regime, we carried out micromagnetic simulations, using MUMAX3 [45] (see [32] for details on the procedure). The chosen dimensional parameters correspond to a ferrimagnetic material with a low M_s and K_u (see Fig. 4 caption). In Fig. 4, we present the skyrmion radius (a) and rotation angle (b) predicted by our model [see (6) and (5)] for this set of parameters. The corresponding values of the skyrmion radius and angle from the simulations are presented, respectively, in Figs. 4(c) and 4(d), where the dashed line is the line of zero bursting barrier defined in (10). Figure 4(c) also shows several points in the parameter space for which we present the numerical magnetization profiles in Fig. 5. These

profiles agree very well with the suitably rotated and dilated Belavin-Polyakov profiles, consistently with our theoretical predictions.

The simulations and the theory show a good agreement: they both predict, at fixed DMI, an increase of the skyrmion radius from around 20 nm up to bursting as the positive field increases [Figs. 4(a) and 4(c)], and at fixed magnetic field, a reorientation of the skyrmion angle from around 60° to 90° as $\bar{\kappa}$ is decreased to zero [Figs. 4(b) and 4(d)]. This confirms the existence of skyrmions stabilized by a parallel field in the low $|\bar{\kappa}|$ regime.

In the top right part of Figs. 4(c) and 4(d) the white zone corresponds to a region where the skyrmion has burst and the system is homogeneously magnetized in the direction of the positive applied field. The numerical solution persists beyond the dashed line representing the region of existence of our solution. This is expected due to the asymptotic nature of the theory. The numerical solution persists in the form of a less compact profile before bursting occurs. This further extends the predicted range in which skyrmions can be stabilized with the help of a positive field.

Conclusions and perspective. We have derived the magnetic field dependence of the compact skyrmion size and rotation angle, along with its thermal stability, in the presence of DMI and full dipolar interaction. In particular, we obtained a condition for skyrmion bursting at positive magnetic field, which agrees quantitatively with micromagnetic simulations in the regime of compact skyrmions and which may be an invaluable tool for predicting this type of instability. We also established that a balance needs to be found between collapse and bursting energy barriers to optimize the skyrmion stability.

Our analysis reveals that due to the presence of long-range dipolar interaction an increase of the magnetic field applied parallel to the skyrmion core increases the size and stability of a skyrmion similarly to the effect of increasing the DMI strength. A reason why a positive applied field has never been used to stabilize skyrmions so far is that the samples in which skyrmions are observed very often exhibit spontaneous demagnetization in the form of a helicoidal state or a stripe state at zero applied field. This phenomenon occurs in the presence of a large DMI or/and due to long-range demagnetizing effects. In the quest for room temperature nanometer size skyrmions, recent works have focused on ferrimagnetic systems, following some predictions of more stable skyrmions in such system with a low M_s and thicknesses of the order of 5–10 nm [14,27]. In these systems, room temperature stable skyrmions are observed experimentally at zero applied magnetic field [46,47] and they constitute the ideal candidates to observe field-stabilized skyrmions in the regime predicted by our theory.

Lastly, while our study focuses on the collapse and bursting mechanisms in the low effective DMI and thickness regime, it would be interesting to extend our investigation to systems exhibiting more complex mechanisms of thermal instability, as in the case of systems with strong DMI and strong magnetocrystalline anisotropy studied previously in the case of no applied field (see, e.g., [42,48–50]).

Acknowledgments. The work of C.B.M. was supported, in part, by NSF via Grant No. DMS-1908709. T.M.S. was funded by the Deutsche Forschungsgemeinschaft (DFG, German Research Foundation) under Germany's Excellence Strategy EXC 2044-390685587, Mathematics Münster: Dynamics–Geometry–Structure.

[1] S. Mühlbauer, B. Binz, F. Jonietz, C. Pfleiderer, A. Rosch, A. Neubauer, R. Georgii, and P. Böni, Skyrmion lattice in a chiral magnet, Science **323**, 915 (2009).

[2] K. Everschor-Sitte, J. Masell, R. M. Reeve, and M. Kläui, Perspective: Magnetic skyrmions—Overview of recent progress in an active research field, J. Appl. Phys. **124**, 240901 (2018).

[3] A. Fert, N. Reyren, and V. Cros, Magnetic skyrmions: advances in physics and potential applications, Nat. Rev. Mater. **2**, 17031 (2017).

[4] X. Zhang, Y. Zhou, K. M. Song, T.-E. Park, J. Xia, M. Ezawa, X. Liu, W. Zhao, G. Zhao, and S. Woo, Skyrmion-electronics: Writing, deleting, reading and processing magnetic skyrmions toward spintronic applications, J. Phys.: Condens. Matter **32**, 143001 (2020).

[5] Y. Tokura and N. Kanazawa, Magnetic skyrmion materials, Chem. Rev. **121**, 2857 (2021).

[6] A. N. Bogdanov and D. A. Yablonskii, Thermodynamically stable "vortices" in magnetically ordered crystals. The mixed state of magnets, J. Exp. Theor. Phys. **68**, 101 (1989).

[7] A. N. Bogdanov, M. V. Kudinov, and D. A. Yablonskii, Theory of magnetic vortices in easy-axis ferromagnets, Sov. Phys. - Solid State **31**, 1707 (1989).

[8] A. Bogdanov and A. Hubert, Thermodynamically stable magnetic vortex states in magnetic crystals, J. Magn. Magn. Mater. **138**, 255 (1994).

[9] A. Bogdanov and A. Hubert, The properties of isolated magnetic vortices, Phys. Status Solidi B **186**, 527 (1994).

[10] A. Bogdanov and A. Hubert, The stability of vortex-like structures in uniaxial ferromagnets, J. Magn. Magn. Mater. **195**, 182 (1999).

[11] C. Melcher, Chiral skyrmions in the plane, Proc. R. Soc. London, Ser. A **470**, 20140394 (2014).

[12] B. Dupé, M. Hoffmann, C. Paillard, and S. Heinze, Tailoring magnetic skyrmions in ultra-thin transition metal films, Nat. Commun. **5**, 4030 (2014).

[13] A. Siemens, Y. Zhang, J. Hagemeister, E. Y. Vedmedenko, and R. Wiesendanger, Minimal radius of magnetic skyrmions: Statics and dynamics, New J. Phys. **18**, 045021 (2016).

[14] F. Büttner, I. Lemesh, and G. S. D. Beach, Theory of isolated magnetic skyrmions: From fundamentals to room temperature applications, Sci. Rep. **8**, 4464 (2018).

[15] X. S. Wang, H. Y. Yuan, and X. R. Wang, A theory on skyrmion size, Commun. Phys. **1**, 31 (2018).

[16] L. Desplat, C. Vogler, J. V. Kim, R. L. Stamps, and D. Suess, Path sampling for lifetimes of metastable magnetic skyrmions and direct comparison with Kramers' method, Phys. Rev. B **101**, 060403(R) (2020).

[17] N. Romming, C. Hanneken, M. Menzel, J. E. Bickel, B. Wolter, K. von Bergmann, A. Kubetzka, and R. Wiesendanger,

Writing and deleting single magnetic skyrmions, Science **341**, 636 (2013).
[18] N. Nagaosa and Y. Tokura, Topological properties and dynamics of magnetic skyrmions, Nat. Nanotechnol. **8**, 899 (2013).
[19] N. Romming, A. Kubetzka, C. Hanneken, K. von Bergmann, and R. Wiesendanger, Field-dependent size and shape of single magnetic skyrmions, Phys. Rev. Lett. **114**, 177203 (2015).
[20] L. Mougel, P. M. Buhl, R. Nemoto, T. Balashov, M. Hervé, J. Skolaut, T. K. Yamada, B. Dupé, and W. Wulfhekel, Instability of skyrmions in magnetic fields, Appl. Phys. Lett. **116**, 262406 (2020).
[21] M. Hervé, B. Dupé, R. Lopes, M. Böttcher, M. D. Martins, T. Balashov, L. Gerhard, J. Sinova, and W. Wulfhekel, Stabilizing spin spirals and isolated skyrmions at low magnetic field exploiting vanishing magnetic anisotropy, Nat. Commun. **9**, 1015 (2018).
[22] N. S. Kiselev, A. N. Bogdanov, R. Schäfer, and U. K. Rößler, Chiral skyrmions in thin magnetic films: New objects for magnetic storage technologies? J. Phys. D: Appl. Phys. **44**, 392001 (2011).
[23] A. Bernand-Mantel, L. Camosi, A. Wartelle, N. Rougemaille, M. Darques, and L. Ranno, The skyrmion-bubble transition in a ferromagnetic thin film, SciPost Phys. **4**, 027 (2018).
[24] F. Tejo, A. Riveros, J. Escrig, K. Y. Guslienko, and O. Chubykalo-Fesenko, Distinct magnetic field dependence of Néel skyrmion sizes in ultrathin nanodots, Sci. Rep. **8**, 6280 (2018).
[25] T. B. Winkler, K. Litzius, A. de Lucia, M. Weißenhofer, H. Fangohr, and M. Kläui, Skyrmion states in disk geometry, Phys. Rev. Appl. **16**, 044014 (2021).
[26] D. Cortés-Ortuño, N. Romming, M. Beg, K. von Bergmann, A. Kubetzka, O. Hovorka, H. Fangohr, and R. Wiesendanger, Nanoscale magnetic skyrmions and target states in confined geometries, Phys. Rev. B **99**, 214408 (2019).
[27] A. Bernand-Mantel, C. B. Muratov, and T. M. Simon, Unraveling the role of dipolar versus Dzyaloshinskii-Moriya interactions in stabilizing compact magnetic skyrmions, Phys. Rev. B **101**, 045416 (2020).
[28] I. S. Lobanov, H. Jonsson, and V. M. Uzdin, Mechanism and activation energy of magnetic skyrmion annihilation obtained from minimum energy path calculations, Phys. Rev. B **94**, 174418 (2016).
[29] C. B. Muratov and V. V. Slastikov, Domain structure of ultrathin ferromagnetic elements in the presence of Dzyaloshinskii-Moriya interaction, Proc. R. Soc. London, Ser. A **473**, 20160666 (2016).
[30] H. Knüpfer, C. B. Muratov, and F. Nolte, Magnetic domains in thin ferromagnetic films with strong perpendicular anisotropy, Arch. Ration. Mech. Anal. **232**, 727 (2019).
[31] C. B. Muratov, A universal thin film model for Ginzburg-Landau energy with dipolar interaction, Calc. Var. Partial Differ. Equations **58**, 52 (2019).
[32] See Supplemental Material at http://link.aps.org/supplemental/10.1103/PhysRevB.108.L161405 for model derivation and details of the micromagnetic simulations.
[33] E. H. Lieb and M. Loss, *Analysis* (American Mathematical Society, Providence, RI, 2010).
[34] A. Hubert and R. Schäfer, *Magnetic Domains* (Springer, Berlin, 1998).
[35] G. D. Chaves-O'Flynn, G. Wolf, J. Z. Sun, and A. D. Kent, Thermal stability of magnetic states in circular thin-film nanomagnets with large perpendicular magnetic anisotropy, Phys. Rev. Appl. **4**, 024010 (2015).
[36] S. Rohart and A. Thiaville, Skyrmion confinement in ultrathin film nanostructures in the presence of Dzyaloshinskii-Moriya interaction, Phys. Rev. B **88**, 184422 (2013).
[37] H.-B. Braun, Topological effects in nanomagnetism: From superparamagnetism to chiral quantum solitons, Adv. Phys. **61**, 1 (2012).
[38] A. Bernand-Mantel, C. B. Muratov, and T. M. Simon, A quantitative description of skyrmions in ultrathin ferromagnetic films and stability of degree ± 1 harmonic maps from $\mathbb{R}^2$ to $\mathbb{S}^2$, Arch. Ration. Mech. Anal. **239**, 219 (2021).
[39] A. A. Belavin and A. M. Polyakov, Metastable states of two-dimensional isotropic ferromagnets, JETP Lett. **22**, 245 (1975).
[40] R. M. Corless, G. H. Gonnet, D. E. G. Hare, D. J. Jeffrey, and D. E. Knuth, On the Lambert *W* function, Adv. Comput. Math. **5**, 329 (1996).
[41] P. F. Bessarab, V. M. Uzdin, and H. Jonsson, Method for finding mechanism and activation energy of magnetic transitions, applied to skyrmion and antivortex annihilation, Comput. Phys. Commun. **196**, 335 (2015).
[42] D. Cortés-Ortuño, W. Wang, M. Beg, R. A. Pepper, M.-A. Bisotti, R. Carey, M. Vousden, T. Kluyver, O. Hovorka, and H. Fangohr, Thermal stability and topological protection of skyrmions in nanotracks, Sci. Rep. **7**, 4060 (2017).
[43] M. Hoffmann, G. P. Müller, and S. Blügel, Atomistic perspective of long lifetimes of small skyrmions at room temperature, Phys. Rev. Lett. **124**, 247201 (2020).
[44] A. Bernand-Mantel, C. B. Muratov, and V. V. Slastikov, A micromagnetic theory of skyrmion lifetime in ultrathin ferromagnetic films, Proc. Natl. Acad. Sci. USA **119**, e2122237119 (2022).
[45] A. Vansteenkiste, J. Leliaert, M. Dvornik, M. Helsen, F. Garcia-Sanchez, and B. Van Waeyenberge, The design and verification of MuMax3, AIP Adv. **4**, 107133 (2014).
[46] L. Caretta, L. Mann, F. Büttner, K. Ueda, B. Pfau, C. M. Günther, P. Hessing, A. Churikova, C. Klose, M. Schneider, D. Engel, C. Marcus, D. Bono, K. Bagschik, S. Eisebitt, and G. S. D. Beach, Fast current-driven domain walls and small skyrmions in a compensated ferrimagnet, Nat. Nanotechnol. **13**, 1154 (2018).
[47] Y. Quessab, J.-W. Xu, E. Cogulu, S. Finizio, J. Raabe, and A. D. Kent, Zero-field nucleation and fast motion of skyrmions induced by nanosecond current pulses in a ferrimagnetic thin film, Nano Lett. **22**, 6091 (2022).
[48] L. Desplat, D. Suess, J. V. Kim, and R. L. Stamps, Thermal stability of metastable magnetic skyrmions: Entropic narrowing and significance of internal eigenmodes, Phys. Rev. B **98**, 134407 (2018).
[49] B. Heil, A. Rosch, and J. Masell, Universality of annihilation barriers of large magnetic skyrmions in chiral and frustrated magnets, Phys. Rev. B **100**, 134424 (2019).
[50] A. S. Varentcova, S. von Malottki, M. N. Potkina, G. Kwiatkowski, S. Heinze, and P. F. Bessarab, Toward room-temperature nanoscale skyrmions in ultrathin films, npj Comput. Mater. **6**, 193 (2020).